Journal of Materials Chemistry A

Accepted Manuscript

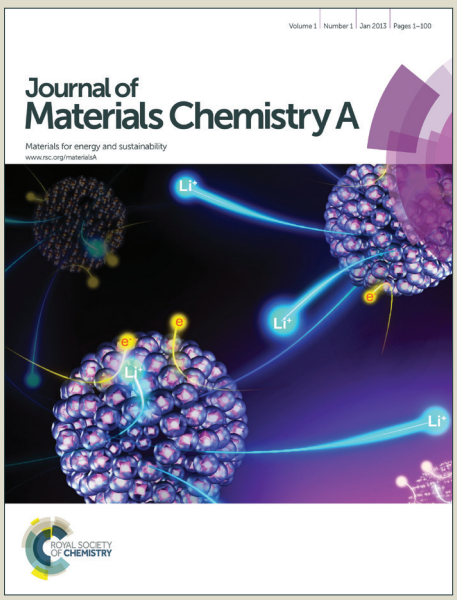

ROYAL SOCIETY OF CHEMISTRY

www.rsc.org/materialsA

Electrochemical and Raman Spectroscopy Identification of Morphological and Phase Transformations in Nanostructured TiO_2(B)

Anthony G. Dylla and Keith J. Stevenson*

Department of Chemistry, University of Texas at Austin, Austin, TX, USA.

Keywords: TiO_2(B), titania, lithium ion battery, anode, intercalation, pseudocapacitor

*Corresponding Author: stevenson@cm.utexas.edu

Abstract

TiO_2(B) exhibits unique electrochemical lithiation behavior where two closely spaced reduction and oxidation peaks, referred to as "double peaks," are observed for 3-D forms of bulk and nanostructured TiO_2(B) while a single broad redox peak is observed for 2-D nanosheet architectures. In this study, we have used a combination of transmission electron micrscopy (TEM), powder X-ray diffraction (XRD), Raman spectroscopy and cyclic voltammetry on TiO_2(B) nanosheets as well as a series of thermally annealed nanosheets to map the morphological and phase transformation pathways that help clarify the structure-dependent lithiation behavior. We found that the double peak redox behavior only arises once a three

dimensional nanocrystalline structure of TiO_2(B) exists by observing nanoparticle growth on the TiO_2(B) nanosheet surface via TEM at temperatures above 150 °C. This morphological transformation was also verified by Raman spectroscopy. The appearance of low-energy torsional modes at temperatures above 150 °C which are not observed in 2-D morphologies of TiO_2(B) agrees well with TEM evidence of 3-D nanoparticle formation. Using scan rate dependent cyclic voltammetry we also verified that all lithiation behavior associated with TiO_2(B) (either nanosheet or nanoparticle) is due primarily to a surface redox (pseudocapacitive) mechanism. The thermal annealing study also shows the phase transformation of surface nucleated TiO_2(B) nanoparticles to anatase nanoparticles at temperatures above 200 °C. These studies clearly show how nano-morphological control can influence electrochemical lithiation behavior and help identify a possible mechanism to explain the double peak phenomenon observed for TiO_2(B).

Introduction

A key factor for the development of high rate and high capacity electrochemical energy storage devices such as rechargeable lithium ion batteries will be to understand how charge storage mechanisms are affected by both phase and nano-morphological control of relevant lithium insertion materials.[1] The nanostructuring of various phases of TiO_2 such as rutile[2,3], anatase[4-7] and most recently, TiO_2(B)[8-12], has been shown to improve their rate capability and specific capacity as Li^+ intercalation anode materials. Nanostructuring these intercalation materials shortens Li^+ diffusion pathways, which helps negate slow solid-state Li^+ diffusion. Additionally, different surface energies and high surface areas afforded by nanostructuring allows for more facile Li^+ insertion.

For the purposes of studying the effects of nanostructuring on electrochemical lithiation mechanisms, TiO_2(B) is a particularly interesting model system as it can be prepared as nanowires[13], nanotubes[11], nanoparticles[9], mesoporous architectures[14] and nanosheets.[15] Kavan and coworkers initially identified lithiation redox peaks in the cyclic voltammetry of nanostructured anatase as "S" or surface peaks related to an amorphous phase of titania.[16] Later, Zukalova and coworkers identified the S peaks as TiO_2(B).[17] They found that bulk TiO_2(B) lithiates and delithiates in the 1.4-1.75 V vs Li/Li^+ range with a distinctive "double peak" redox behavior and were the first to identify a pseudocapacitive charging mechanism for TiO_2(B) using scan rate dependent cyclic voltammetry. The closely spaced (<100 mV) reduction and oxidation double peaks were hypothesized to be two distinct lithiation sites or two ordered superstructures of lithiated TiO_2(B).[18] Since this report, the double peak phenomenon has consistently been observed for various nanostructures of TiO_2(B). We have recently shown in a combined experimental and DFT+U study that nanostructuring TiO_2(B) influences the lithiation mechanism and provided some clues to further understanding the double peak phenomenon.[15] Ultra-thin (~1 nm) nanosheets of TiO_2(B) exhibited a highly broadened redox envelope rather than the distinct redox peaks observed for the lithiation of bulk and nanoparticle forms of TiO_2(B) and the DFT+U calculated lithiation/delithiation potentials for the 2-D (nanosheet) versus 3-D (bulk and nanoparticle) TiO_2(B) qualitatively matched the experimental data. The calculations for the 3-D TiO_2(B) (bulk and nanoparticle) showed that Li^+ resides near axial and equatorial oxygens of the TiO_6 octahedral crystalline framework of TiO_2(B) that are commonly labeled A1 and A2, respectively, while C-site (open channel along the b-axis) occupation is not energetically stable. The calculations suggest that all of the A2 sites are filled at 1.54 V vs Li/Li^+ followed by half of A1 site filling at 1.5 V. These calculations are consistent with the observed

double peak phenomenon and the peak splitting potential difference supports the specific site filling hypothesis. In contrast, the calculation for the 2-D nanosheet architecture showed a range of Li^+ site filling potentials that start at 2.05 V and incrementally fill C-sites and off-axis A1 sites down to 1.04 V. The calculated crystal structure for TiO_2(B) nanosheets showed relaxation along the a-axis that shortened the distance between neighboring axial oxygens that allows energetically favorable C-site lithiation.

In this work, we have set out to test this hypothesis by systematically transforming 2-D TiO_2(B) nanosheets into 3-D nanoparticles via incremental thermal treatments and use transmission electron microscopy (TEM), powder X-ray diffraction (XRD), Raman and cyclic voltammetry to characterize the changes in architecture, phase and lithiation mechanism. Specifically, cyclic voltammetry of the lithiation/delithiation process provides a sensitive probe of both the nano-morphology and phase of the titania. The results presented below demonstrate that the double peak phenomenon is related to three dimensional architectures of TiO_2(B). Thermally assisted growth of 3-D nanocrystalline particles within the nanosheet domain correlate with a change from a broad redox envelope to the double peak lithiation observed in cyclic voltammetry. Upon further heating a portion of the TiO_2(B) nanoparticles transform into anatase nanoparticles that are readily identified by their lithiation/delithiation redox couple at 1.65 V (lithiation) and 2.1 V (delithiation) vs Li/Li^+. The morphology and phase transformations observed in the electrochemical analysis are consistent with TEM and Raman analysis.

Experimental

TiO_2(B) nanosheets (TiO_2(B)-NS) were synthesized using a previous method reported by Xiang et al.[19] Here, 1 mL of $TiCl_3$ (Alfa Aesar, 20% in 3% HCl) and 1 mL of H_2O (Nanopure, 18 MΩ cm) were added to 30 mL of ethylene glycol (Aldrich) in a 100 mL round-bottom flask. This

mixture was slowly stirred at 150 °C for 3 h open to air. The off-white-colored product was washed several times with ethanol (Fisher) followed by centrifugation and drying overnight at 60 °C. Bulk and nanoparticle forms of TiO_2(B) used for comparative purposes were synthesized from previously reported literature methods.[20,21] Anatase powders were obtained from Fisher.

To study architecture and morphology changes, the TiO_2(B)-NS powders were heated in a tube furnace under flowing air atmosphere and held at specified temperatures (100, 150, 200, 250, 300 and 350 °C) for 3 hours before allowing the reactor to cool slowly to room temperature. These samples are hereafter referred to as TiO_2-100, TiO_2-150, TiO_2-200, TiO_2-250 and TiO_2-300. The powders were used directly for further analysis.

The titania powders were characterized by TEM (Jeol 2010F operated at 200 kV), XRD (Rigaku Spider, Cu Ka radiation, λ = 1.5418 Å), Raman spectroscopy (Renishaw InVia microscope with a 514 nm Ar^+ laser operated below 4 mW), and thermogravimetric analysis TGA (Mettler-Toledo, 10 °C/min ramp rate from 25 to 600 °C in air atmosphere). Electrochemical measurements were performed using a CHI 660D potentiostat inside an MBraun glovebox with <0.1 ppm H_2O and <1 ppm O_2. The titania powders were directly deposited onto fluorine-doped tin oxide (FTO) conductive substrates from an ethanol slurry. Lithium metal foil (Fisher) served as both counter and reference electrodes, the titania-coated FTO served as the working electrode with cyclic voltammetry data normalized to the electrode surface area (38 mm^2), and 1.0 M $LiPF_6$ in ethylene carbonate / diethylene carbonate EC:DEC (1:1) v/v (Novalyte Technologies) was used as the electrolyte.

Results & Discussion

TiO_2(B) nanosheets (TiO_2(B)-NS) were synthesized using a previously reported method described in the experimental section. Figure 1a and 1b show transmission electron microscopy

(TEM) of as synthesized TiO_2(B)-NS and TiO2-100, respectively, which exhibit a flexible sheet like morphology as observed by the buckling and folding with the sheets ranging in size up to 500 nm diameter. High resolution TEM (HR-TEM) of the as synthesized TiO_2(B)-NS and TiO_2-100 (Fig. 2a and 2b) show that although the sheet structures are flexible, they contain small domains of crystallinity that index to the (020) facet of TiO_2(B). Upon thermal annealing ~2 nm diameter particles begin to decorate the surface of the nanosheets as can be seen in the TiO_2-150 sample (Fig. 1c). HR-TEM of TiO_2-150 (Fig. 2c) shows nanocrystalline domains within the plane of the sheet morphology that are

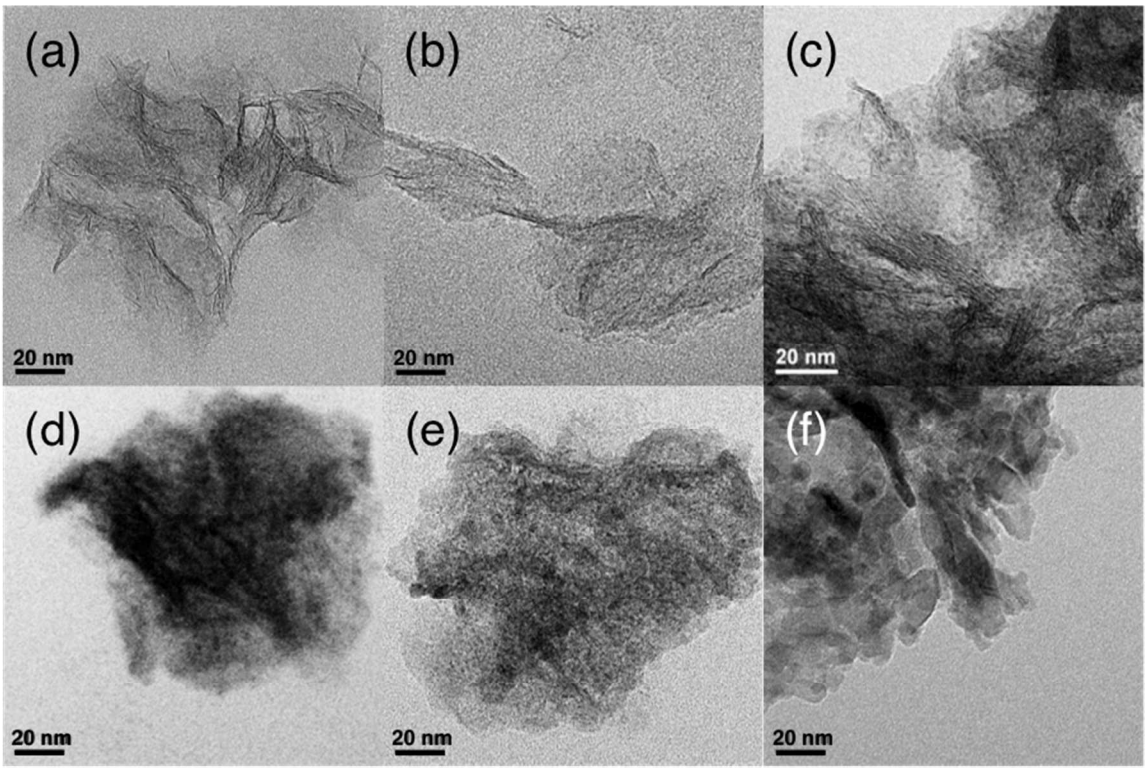

Figure 1. TEM of as synthesized (a) and thermally treated TiO_2(B)-NS: TiO_2-100 (b), TiO_2-150 (c), TiO_2-200 (d), TiO_2-250 (e) and TiO_2-300 (f).

consistent with the (003) facet of TiO_2(B). Upon further heat treatment to 200 °C (TiO_2-200) surface bound ethylene glycol remaining from synthesis is degraded into carbonaceous deposits

on the surface as can be observed in Figures 1d and 2d. The thermal degradation of ethylene glycol is consistent with TGA (S.I. 1) as well as Raman results to be discussed later. At 250 °C, further growth in particle size and increased crystallinity is observed (Figs. 1e and 2e). Finally, at 300 °C elongated TiO_2(B) particles of approximately 40 nm in length and <10 nm in diameter are clearly seen on the surface of the nanosheet (Fig. 1f) with (001) facets exposed along with 5-10 nm anatase spherical particles identified by (101) facets (Fig. 2f). TiO_2(B) nanosheets synthesized under similar conditions are reported to have thicknesses of 1-2 nm indicating nearly atomically thin sheet structures with the

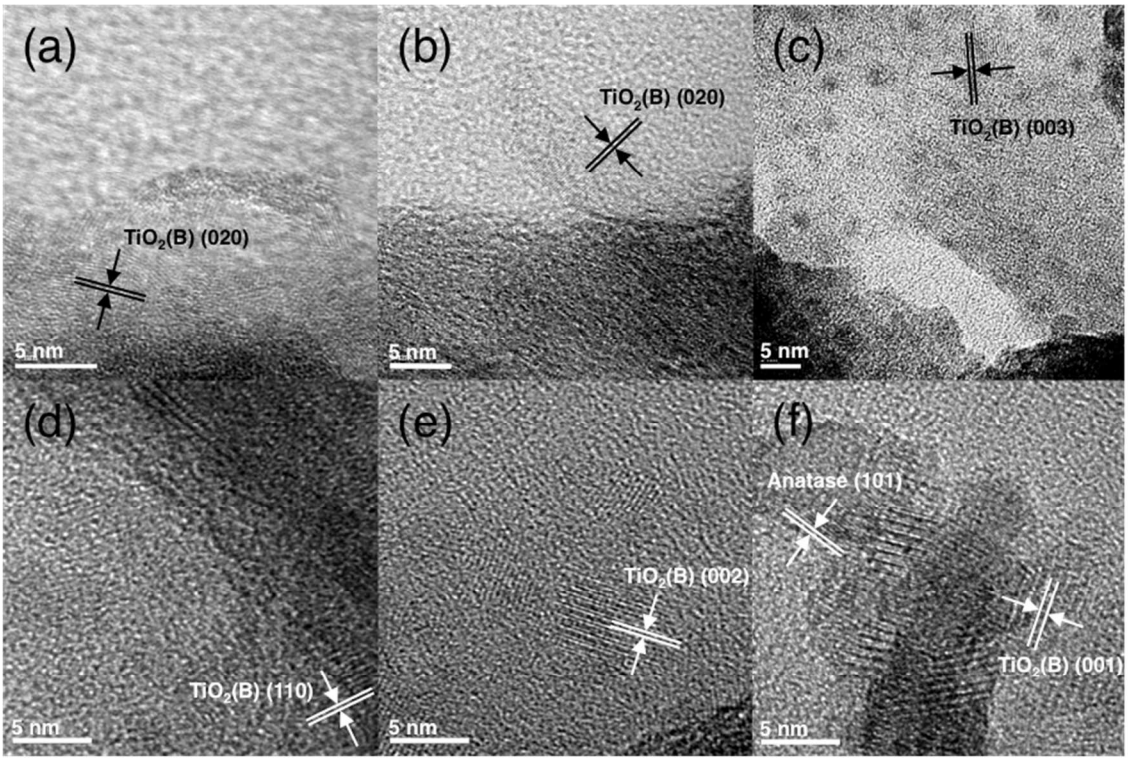

Figure 2. HR-TEM of as synthesized (a) and thermally treated TiO_2(B)-NS: TiO_2-100 (b), TiO_2-150 (c), TiO_2-200 (d), TiO_2-250 (e) and TiO_2-300 (f).

(001) plane as the terminus for a single layer.[19] Observation of the (001) facet indicates that 3-D growth has occurred. Furthermore, elongated TiO_2(B) nanoparticle growth is consistent with the

needle-like morphologies observed in bulk TiO_2(B).[22] These results suggest that TiO_2(B) nanosheets self-nucleate particles of TiO_2(B) followed by growth of both TiO_2(B) nanoparticles as well as conversion to anatase nanoparticles. Anatase is a common contaminant of many TiO_2(B) syntheses due to TiO_2(B) being a meta-stable phase.[21] This result also demonstrates that conversion of TiO_2(B) to anatase occurs through particle conversion rather than nanosheets collapsing directly to 3-D bulk or nanoparticulate morphologies of anatase.

X-ray diffraction (XRD) was used to monitor and identify crystalline phase transformations of TiO_2(B) during thermal annealing and is presented in Figure 3. XRD of TiO_2(B)-NS (Fig. 3 'RT') exhibits an enhanced (020):(110) relative peak ratio due to the preferential flat alignment

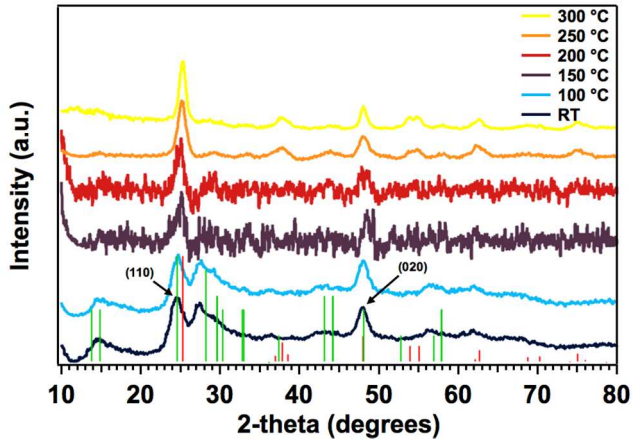

Figure 3. XRD of as synthesized and thermally treated TiO_2(B)-NS. Vertical red and green lines indicate ideal diffraction patterns of anatase (JCPDS: 202242) and TiO_2(B) (JCPDS: 741940), respectively.

of the sheet architecture that is consistent with previous reports.[19] Besides the (110) and (020) peaks, all other diffraction peaks diminish as the temperature is increased to 150 and 200 °C. This may be indicative of the formation of a carbon coating on the surface (see TGA in S.I. 1) and thereby reducing the diffraction efficiency. Finally, the anatase phase can be clearly

identified by the (103), (004) and (112) peaks along with TiO_2(B) diffraction peaks as the temperature reaches ≥250 °C. Unfortunately TiO_2(B) and anatase have many overlapping diffraction peaks and the nano-scale of the TiO_2(B) creates peak broadening which makes further analysis difficult.

Raman spectroscopy is a useful tool for characterizing titania phases due to the highly variable local bonding structure of the different morphologies as well as being able to identify non-crystalline phases and surface carbon adsorbates that may be unobservable in XRD analysis. Figure 4a shows *in situ* Raman of the TiO_2(B)-NS along with *ex situ* comparisons of selected annealing temperatures with standards (Fig. 4b). The Raman spectrum of TiO_2(B)-NS

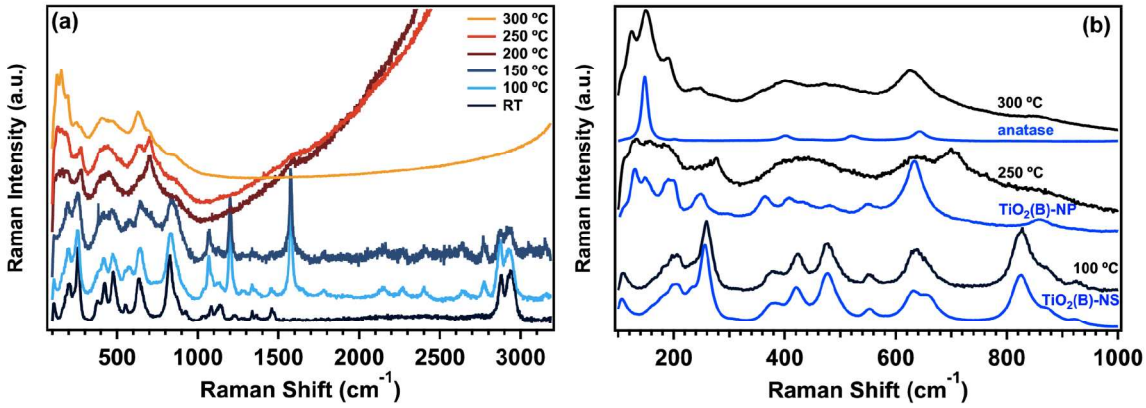

Figure 4. Raman spectra of as synthesized and thermally treated TiO_2(B)-NS (a) and a comparison of three temperature regimes to reference materials (b).

(Fig. 4a 'RT') is consistent with our previous report using similar synthesis methods.[15] Additionally, C-H symmetric and antisymmetric stretching modes observed at 2850-2950 cm^{-1} are indicative of surface adsorbed ethylene glycol remaining from the synthesis of TiO_2(B)-NS. At 100 °C a new peak appears at 1577 cm^{-1} that is due to surface adsorbed ethylene glycol decomposition to form graphitic carbon deposits. Raman spectra of carbonaceous materials with a strong G-peak (~1580 cm^{-1}) relative to the D-peak (~1320 cm^{-1}) is typical for large domain

graphite deposits identified by symmetric stretching of sp^2 hybridized carbon.[23] Several distinct changes in the spectra occur as the temperature is raised to 200 °C and 250 °C. First, the distinct G-band observed at 100 and 150 °C is significantly diminished indicating further decomposition of ethylene glycol into surface carbon deposits. Secondly, the baseline is severely sloped in both the 200 and 250 °C spectrum, which is likely due to fluorescence from newly formed polymeric carbon deposits. Finally, two new peaks are identified at 128 and 145 cm^{-1}. In previous work, we identified distinct Raman modes for nanoparticle (3-D) and nanosheet (2-D) architectures of TiO_2(B).[15] The TiO_2(B)-NS spectrum is quite similar to TiO_2(B)-NP and bulk spectra from 200 to 700 cm^{-1} but deviates significantly below 200 cm^{-1} as several of the low-energy Ti−O−Ti and O−Ti−O torsional modes are absent at ~130 and ~150 cm^{-1}. The absence of peaks may be due to dimensional constraint of the 2-D architecture of TiO_2(B)-NS causing these low energy modes to be Raman inaccessible. These differences can be seen clearly in Figure 4b where several of the *in situ* Raman spectra from Figure 4a are compared to TiO_2(B)-NS, TiO_2(B)-NP and anatase standards. While poorly defined, the new peaks at 128 and 145 cm^{-1} in the '200' and '250' spectra clearly identify Raman modes associated with 3-D forms of TiO_2(B). This result is consistent with the TEM analysis presented in Figures 1 and 2. Finally, at 300 °C the *in situ* Raman spectrum shows diminished fluorescence due to carbon burn off (see TGA in S.I. 1) and new peaks appear due to anatase formation (see Fig. 4b) as well as peaks from 3-D TiO_2(B).

Scan rate dependent CV of lithiation/delithiation cycling of TiO_2(B)-NS and thermally treated samples is presented in Figure 5. As mentioned previously, electrochemical lithiation and delithiation of bulk and nanoparticulate TiO_2(B) gives two closely spaced peaks centered near 1.45 and 1.65 V vs Li/Li^+, respectively, while TiO_2(B) nanosheets lithiate and delithiate over a broad range of potentials: 1.6 to 1.0 V vs Li/Li^+ for lithiation and 1.5 to 2.0 V vs Li/Li^+ for

delithiation. Along with identifying lithiation redox potentials, CV can also been used to determine the primary charge storage mechanism of many relevant Li^+ insertion materials.[24] The two general charge storage mechanisms are diffusion limited Li^+ insertion typical of bulk materials and pseudocapacitive Li^+ insertion, which is a surface redox process that is often observed in nanomaterials where surface or interfacial processes dominate. Scan rate dependent CV can be used to determine these mechanism by equations (1) and (2) below:

$$i = 0.4958nFAc\left(\frac{D\alpha nF\nu}{RT}\right)^{1/2} \quad (1)$$

$$i = \frac{dV}{dt}C_{\Phi} = \nu C_{\Phi} \quad (2)$$

where i is the peak current, n is the number of electrons, F is the Faraday constant, A is the electrode area, c is the concentration, D is the diffusion coefficient, α is the transfer coefficient, R is the gas constant, T is the temperature, C_{Φ} is surface capacitance and ν is the scan rate.[25,26]

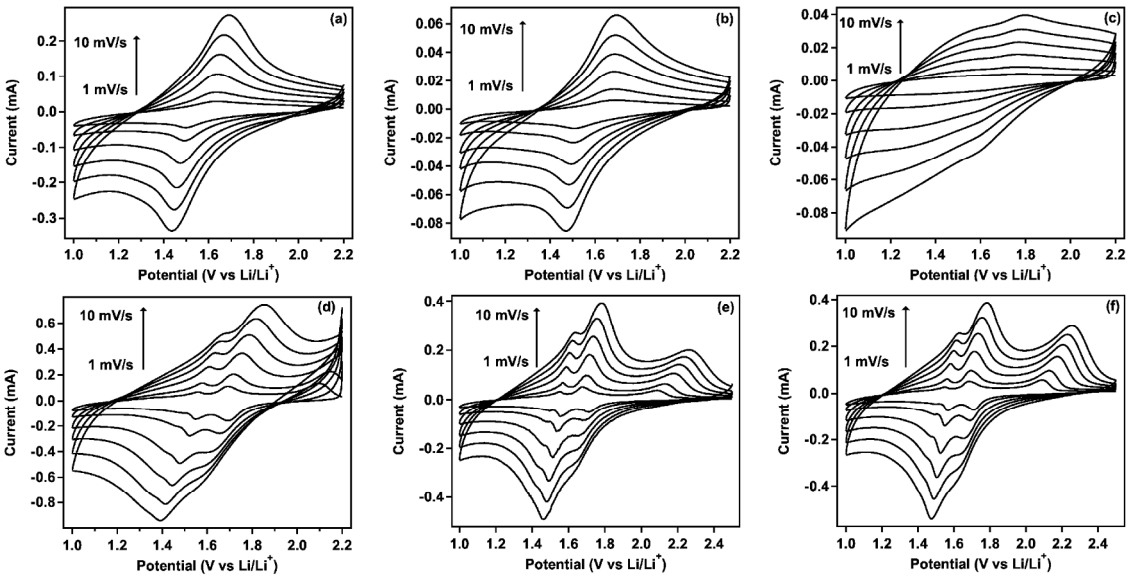

Figure 5. Cyclic voltammetry at a series of scan rates for as synthesized (a) and thermally treated TiO_2(B)-NS: TiO_2-100 (b), TiO_2-150 (c), TiO_2-200 (d), TiO_2-250 (e) and TiO_2-300 (f).

Equation (1) describes current due to normal diffusion controlled Faradaic Li^+ insertion processes where the current is linear with respect to the square root of scan rate and equation (2) describes pseudocapacitive current due to surface processes where the current is linear with respect to scan rate. TiO_2(B) is a unique material in that even the bulk appears to lithiate through a pseudocapacitive mechanism as described by Kavan et al.[16]

Figure 5a shows scan rate dependent CVs for the TiO_2(B)-NS. The electrochemical lithiation/delithiation response shows similar redox behavior to previously reported galvanostatic cycling data in terms of lithiation and delithiation peak voltages, 1.45 and 1.65 V vs Li/Li^+, respectively, as well as the broad overall shape.[15] Little change is observed in the CV of the TiO_2-100 sample shown in Figure 5b. The CV changes significantly at 150 °C (Fig. 5c) as the shape becomes less defined likely due to interference from carbon coating. Also, two peaks (1.55 and 1.75 V) can be identified during the delithiation (oxidative) sweep indicating that a more crystalline nanoparticle structure of TiO_2(B) has been formed. The carbon formation and crystalline TiO_2(B) nanoparticle formation are both consistent with the TEM and Raman results. Upon heating to 200 °C (Fig. 5d) the CV begins to exhibit a redox couple consistent with lithiation and delithiation of anatase at 1.7 and 2.1 V, respectively, along with the double peak lithiation and delithiation typical of 3-D structures of TiO_2(B) at lower voltages. This result is corroborated with the Raman spectrum of TiO_2-200 that shows the low energy (<200 cm^{-1}) Ti-O-Ti and O-Ti-O torsional modes of TiO_2(B) that are not observed for TiO_2(B)-NS. The CVs for the 250 and 300 °C treated samples (Fig. 5e and f) show increasing degree of anatase while the TiO_2(B) double peaks become more well defined. A possible reason that we did not observe crystalline anatase particles in TEM at 200 °C and 250 °C is due to limited sampling space compared to a thin-film areal electrode.

Along with determining the lithiation and delithiation redox response, we also used scan rate dependent CVs to determine the primary charge storage mechanisms of the various thermally annealed samples. Figure 6 shows the peak reduction (lithiation) current vs. scan rate for TiO_2(B)-NS as well as thermally treated samples. All of the TiO_2(B) reduction peaks are linear with respect to scan rate suggesting that pseudocapacitive surface charging is the dominant charge storage mechanism for both nanosheets and nanoparticles. This result is consistent with other reports of pseudocapacitve charge storage in various TiO_2(B) nanostructures as well as bulk.[8,17] The anatase reduction

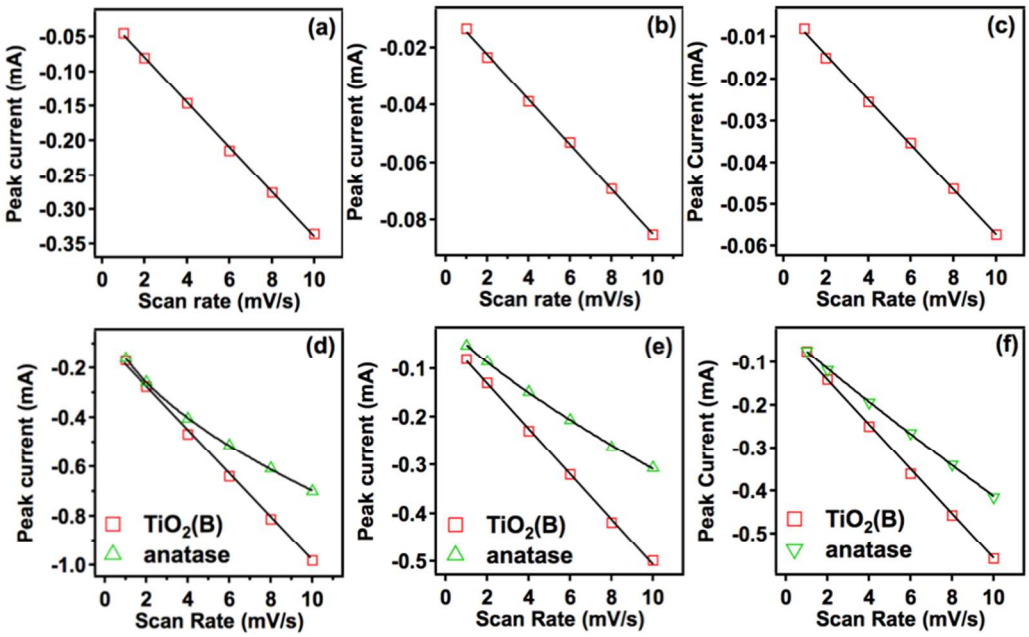

Figure 6. Scan rate dependence of peak reduction (lithiation) current for as synthesized (a) and thermally treated TiO_2(B)-NS: TiO_2-100 (b), TiO_2-150 (c), TiO_2-200 (d), TiO_2-250 (e) and TiO_2-300 (f). Red squares and green triangles indicate TiO_2(B) and anatase, respectively.

peak seen in Figure 6d, e and f does not track linearly with scan rate or with square root of scan rate suggesting that a combination of mechanisms may be contributing to lithium charge storage

in anatase particles. Dunn and coworkers used a similar scan rate dependence analysis to determine that as the size of anatase nanoparticles decreased from 30 nm to 7 nm, the amount of charge storage due to pseudocapacitance increased, but even 7 nm particles still showed ~40% diffusion limited charge storage.[4]

Conclusions

We have used a combination of TEM, XRD, Raman spectroscopy and cyclic voltammetry on TiO_2(B) nanosheets as well as a series of thermally annealed nanosheets to show a morphology and phase transformation pathway that also verifies the structure-dependent lithiation/delithiation behavior. We found that the double peak redox behavior only arises once a three dimensional nanocrystalline structure of TiO_2(B) exists by observing nanoparticle growth on the TiO_2(B) nanosheet surface via TEM. Using scan rate dependent cyclic voltammetry we also verified that all redox behavior associated with TiO_2(B) (either nanosheet or nanoparticle) is due primarily to a surface redox (pseudocapacitive) mechanism. The thermal annealing study also shows the transformation of surface nucleated TiO_2(B) nanoparticles to anatase nanoparticles at temperatures above 200 °C. This work also shows the power of cyclic voltammetry to study electrochemical lithiation/delithation mechamisms as it can be useful as a reporter on nanomorphology and phase as well as being able to identify charge storage processes.

Associated Content

Thermal gravimetric analysis (TGA) of TiO_2(B) nanosheets under inert and oxidizing atmospheres is available in the supporting information. This material is available free of charge via the Internet.

Acknowledgement

This material is based upon work supported as part of the program "Understanding Charge Separation and Transfer at Interfaces in Energy Materials (EFRC:CST)", an Energy Frontier Research Center funded by the U.S. Department of Energy, Office of Science, Office of Basic Energy Sciences under Award Number DE-SC0001091. KJS acknowledges the Welch Foundation (Grant F-1529) for additional funding.

References

1. Maier, J. Pushing Nanoionics to the Limits: Charge Carrier Chemistry in Extremely Small Systems. *Chem. Mater.* **2013**, *26*, 348-360.

2. Hu, Y.-S.; Kienle, L.; Guo, Y.-G.; Maier, J. High Lithium Electroactivity of Nanometer-Sized Rutile TiO_2. *Adv. Mater.* **2006**, *18*, 1421–1426.

3. Qiao, H.; Tao, D.; Wang, Y.; Cai, Y.; Huang, F.; Yang, X.; Wei, J.; Wei, Q. Electrochemical Charge Storage of Flowerlike Rutile TiO_2 Nanorods. *Chem. Phys. Lett.* **2010**, *490*, 180–183.

4. Wang, J.; Polleux, J.; Lim, J.; Dunn, B. Pseudocapacitive Contributions to Electrochemical Energy Storage in TiO_2 (Anatase) Nanoparticles. *J. Phys. Chem. C* **2007**, *111*, 14925–14931.

5. Wagemaker, M.; Borghols, W. J. H.; Mulder, F. M. Large Impact of Particle Size on Insertion Reactions. a Case for Anatase Li_xTiO_2. *J. Am. Chem. Soc.* **2007**, *129*, 4323–4327.

6. Szeifert, J. M.; Feckl, J. M.; Fattakhova-Rohlfing, D.; Liu, Y.; Kalousek, V.; Rathousky, J.; Bein, T. Ultrasmall Titania Nanocrystals and Their Direct Assembly Into Mesoporous Structures Showing Fast Lithium Insertion. *J. Am. Chem. Soc.* **2010**, *132*, 12605–12611.

7. Gentili, V.; Brutti, S.; Hardwick, L. J.; Armstrong, A. R.; Panero, S.; Bruce, P. G. Lithium Insertion Into Anatase Nanotubes. *Chem. Mater.* **2012**, *24*, 4468–4476.

8. Liu, H.; Bi, Z.; Sun, X.-G.; Unocic, R. R.; Paranthaman, M. P.; Dai, S.; Brown, G. M. Mesoporous TiO(2)-B Microspheres with Superior Rate Performance for Lithium Ion Batteries. *Adv. Mater.* **2011**, *23*, 3450–3454.

9. Ren, Y.; Bruce, P. G. Nanoparticulate TiO_2(B): an Anode for Lithium-Ion Batteries. *Angew. Chem. Int. Edit.* **2012**, *51*, 2164–2167.

10. Liu, S.; Jia, H.; Han, L.; Wang, J.; Gao, P.; Xu, D.; Yang, J.; Che, S. Nanosheet-Constructed Porous TiO_2-B for Advanced Lithium Ion Batteries. *Adv. Mater.* **2012**, *24*, 4097-4111.

11. Armstrong, G.; Armstrong, A. R.; Canales, J.; Bruce, P. G. Nanotubes with the TiO_2-B Structure. *Chem. Commun.* **2005**, 2454-2456.

12. Armstrong, A. R.; Armstrong, G.; Canales, J.; Bruce, P. G. TiO_2-B Nanowires. *Angew. Chem. Int. Edit.* **2004**, *43*, 2286–2288.

13. Armstrong, A.; Armstrong, G.; Canales, J.; Garcia, R.; Bruce, P. Lithium-Ion Intercalation Into TiO_2-B Nanowires. *Adv. Mater.* **2005**, *17*, 862–865.

14. Procházka, J.; Kavan, L.; Zukalová, M.; Frank, O.; Kalbáč, M.; Zukal, A.; Klementová, M.; Carbone, D.; Graetzel, M. Novel Synthesis of the TiO_2(B) Multilayer Templated Films. *Chem. Mater.* **2009**, *21*, 1457–1464.

15. Dylla, A. G.; Xiao, P.; Henkelman, G.; Stevenson, K. J. Morphological Dependence of Lithium Insertion in Nanocrystalline TiO_2(B) Nanoparticles and Nanosheets. *J. Phys. Chem. Lett.* **2012**, *3*, 2015-2019.

16. Kavan, L.; Rathouský, J.; Grätzel, M.; Shklover, V.; Zukal, A. Surfactant-Templated TiO_2(Anatase): Characteristic Features of Lithium Insertion Electrochemistry in Organized Nanostructures. *J. Phys. Chem. B* **2000**, *104*, 12012–12020.

17. Zukalova, M.; Kalbac, M.; Kavan, L.; Exnar, I.; Graetzel, M. Pseudocapacitive Lithium Storage in TiO_2(B). *Chem. Mater.* **2005**, *17*, 1248–1255.

18. Zachauchristiansen, B.; West, K.; Jacobsen, T.; Atlung, S. Lithium Insertion in Different TiO_2 Modifications. *Solid State Ionics* **1988**, *28*, 1176–1182.

19. Xiang, G.; Li, T.; Zhuang, J.; Wang, X. Large-Scale Synthesis of Metastable TiO_2(B) Nanosheets with Atomic Thickness and Their Photocatalytic Properties. *Chem. Commun.* **2010**, *46*, 6801–6803.

20. Marchand, R.; Brohan, L.; Tournoux, M. TiO_2(B) a New Form of Titanium-Dioxide and the Potassium Octatitanate $K_2Ti_8O_{17}$. *Mater. Res. Bull.* **1980**, *15*, 1129–1133.

21. Kobayashi, M.; Petrykin, V. V.; Kakihana, M. One-Step Synthesis of TiO_2(B) Nanoparticles From a Water-Soluble Titanium Complex. *Chem. Mater.* **2007**, *19*, 5373–5376.

22. Zukalova, M.; Kalbac, M.; Kavan, L.; Exnar, I.; Haeger, A.; Graetzel, M. Electrochemical and Gas-Phase Photocatalytic Performance of Nanostructured TiO_2(B) Prepared by Novel Synthetic Route. *Prog. Sol. State Chem.* **2005**, *33*, 253–261.

23. Ferrari, A. C.; Robertson, J. Interpretation of Raman Spectra of Disordered and Amorphous Carbon. *Phys. Rev. B* **2000**, *61*, 14095–14107.

24. Lindstrom, H.; Sodergren, S.; Solbrand, A.; Rensmo, H.; Hjelm, J.; Hagfeldt, A.; Lindquist, S. Li^+ Ion Insertion in TiO_2 (Anatase) 2. Voltammetry on Nanoporous Films. *J. Phys. Chem. B* **1997**, *101*, 7717–7722.

25. Bard, A. J.; Faulkner, L. R. *Electrochemical Methods: Fundamentals and Applications*; John Wiley & Sons: New York, 2001.

26. Conway, B. E. Transition From Supercapacitor to Battery Behavior in Electrochemical Energy-Storage. *J. Electrochem. Soc.* **1991**, *138*, 1539–1548.

GRAPHICAL ABSTRACT:

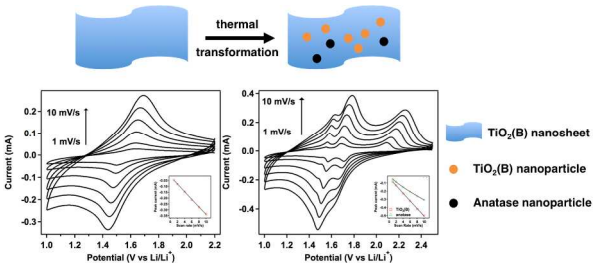

We have systematically studied 2-D TiO_2(B) nanosheets into 3-D nanoparticles using Raman and cyclic voltammetry to characterize changes in lithiation mechanism.